Conclusion

It has been shown that it is possible to stabilize passively the motion of a simplified model of a spinning Skylab by deploying flexible booms, thus altering the moments of inertia. Analytical results indicate the required boom-stiffness properties for given vehicle mass properties and spin rates to achieve passive stability. Furthermore, the use of the simplified model leads to results amenable to physical interpretation.

To gain confidence that these results will apply to the actual Skylab, an additional step is being implemented. A detailed digital simulation model of the spinning Skylab vehicle has been developed at the Marshall Space Fight Center, and results compare favorably with those of the simplified model.

References

[1] Chubb, W. B. and Seltzer, S. M., "Skylab Attitude and Pointing Control System", TND-6068, 1971, NASA.

[2] Siljak, D. D., *Nonlinear Systems*, Wiley, New York, 1969, pp. 4–51, 33–37, 404–406, and 455–457.

[3] Barbera, F. J., "Attitude Stability of Spinning Flexible Spacecraft," Ph.D. dissertation, 1971, Univ. of California, Los Angeles, Calif.

SEPTEMBER 1972 J. SPACECRAFT VOL. 9, NO. 9

Supersonic Dynamic Stability Experiments on the Space Shuttle

K. J. ORLIK-RÜCKEMANN*, J. G. LABERGE† AND E. S. HANFF†
National Aeronautical Establishment,‡ Ottawa, Ontario, Canada

A wind-tunnel study was performed of the longitudinal dynamic stability of the shuttle spacecraft at supersonic speeds. In particular, the study included the determination of the damping-in-pitch characteristics of the orbiter and of the booster, both separately and in a mated launch configuration, and the investigation of the effect of a simulated rocket exhaust plume and of the static and dynamic interference during abort separation. Static interference is defined here as caused by the proximity of the second vehicle when that vehicle is stationary, whereas dynamic interference denotes the same effect, but with the other vehicle performing an oscillatory motion. It was found that, in general, the static interference effects were small, whereas, for the case of the orbiter and the booster performing synchronous oscillations, the dynamic interference effect was very large and could lead to a strongly negative damping of the orbiter.

Introduction

THE unconventional configurations employed for the space shuttle and its often rather unusual flight conditions render the analytical prediction of its aerodynamic characteristics extremely difficult. Thus in many cases the experimental data constitute the sole source of information. One such area where a heavy dependence on experiments is necessary involves the prediction of the dynamic stability characteristics of the shuttle. Although often not of critical importance for the preliminary design, this information usually is required for the complete performance analysis. In addition, there are several flight conditions, such as the ascent of the launch configuration, some phases of the abort separation, and the transitional flight of the orbiter, where the dynamic stability characteristics of the shuttle may very well prove to be significant in the final design and formulation of operational procedures.

This paper describes the dynamic stability experiments on the shuttle, which were performed as part of the internal research program of the National Aeronautical Establishment (NAE). In addition to discussing certain new concepts and new techniques which were specially developed for these experiments, the paper contains a representative selection of dynamic stability results for the shuttle, including certain unusual interference effects such as those occurring during an abort separation and in the presence of an exhaust plume. Oil-flow visualization pictures and high-speed shadowgraph movies are used to illustrate some of the complex flowfields involved in these cases.

Presented as Paper 72-135 at the AIAA 10th Aerospace Sciences Meeting, San Diego, Calif., January 17–19, 1972; submitted January 19, 1972; revision received May 3, 1972.

Index categories: Aircraft Handling, Stability and Control; Aircraft and Component Wind Tunnel Testing.

* Head, Unsteady Aerodynamics Laboratory. Associate Fellow AIAA.

† Research Officers.

‡ A division of the National Research Council of Canada.

Experimental Arrangement

The experiments were performed on 1/360 scale models of the fully reusable shuttle spacecraft, which were manufactured and supplied by NASA Langley Research Center. Models typical of both the low cross-range and the high cross-range configurations were investigated. The former were represented by a straight-wing orbiter and a straight-wing booster, and the latter by a delta-wing orbiter and swept-wing canard booster. Details of the two sets of models are given in Refs. 1–3. The pitching moment derivatives of both orbiters were referred to the total wing area and the wing mean aerodynamic chord, while a scaled-down standard reference area (10,000 ft^2) and reference length (200 ft) were used for the two boosters. The distance of the axis of oscillation (and the moment reference point) from the model nose, referred to the model length, was 0.612 and 0.610 for the straight-wing orbiter and booster, respectively, and 0.456 and 0.465 for the delta-wing orbiter and booster.

For the study of interference effects during abort separation, which constitutes part of this paper, stability derivatives were measured on an oscillating model in the presence of a second model that could either be stationary (causing static interference) or perform a simultaneous oscillatory motion (causing dynamic interference). As discussed at some length in Ref. 4, the most convenient and reliable way to perform the required experiments was to employ the half-model technique. The arrangement of the experimental equipment in the NAE 30-in × 16-in. suction wind tunnel is depicted in Fig. 1. Half-models of the two components of the shuttle spacecraft are mounted very close to a reflection plate, which is displaced about 1 in. from the wind-tunnel wall. The model on which the derivatives are to be measured (orbiter or booster) is attached to an adapter which, in turn, is attached to a cruciform spring in the half-model dynamic balance on the outside of the wind tunnel. An oscillatory motion may be imparted to the model by means of an electromagnetic oscillator which consists of a pair of light-weight coils moving in a magnetic field, while a signal proportional to the angular displacement of the model is obtained from a strain-gage bridge on the spring.

For the static interference experiments, the second model is attached to the reflection plate in such a way that its vertical and longitudinal separation distances and the incidence relative to the first model can be easily varied. The incidence of the whole configuration is varied by rotating the wind-tunnel plate (with the reflection plate). For the dynamic interference experiments, the second model is mounted on a pivot which defines its center of oscillation, while an oscillatory motion of a known amplitude is imparted by means of an eccentric drive connected to a synchronous motor; the two motions can be made synchronous, and the phase relationship between them varied as required.

Details about the free-oscillation and the forced-oscillation methods of derivative measurements, both of which were employed for this program, may be found in Ref. 4. For the dynamic-interference studies, the inclusion of a second oscillating model (which, in this investigation, was always the booster) requires the addition of further circuitry (shown in Fig. 2) where provisions have been made for either synchronous or asynchronous oscillation of the two models.

In the synchronous mode of operation, which is the one of principal interest here, the output signal V_1 from the orbiter displacement transducer is applied to a clipping amplifier whose output is a square wave of fixed amplitude over the complete range of input signal amplitude. The harmonic frequencies of the square wave are eliminated by means of a low-pass filter, and the fundamental component is fed into an adjustable phase shifter whose output is amplified before being applied to the synchronous motor that drives the booster through an eccentric mechanism. Thus, the signal supplied

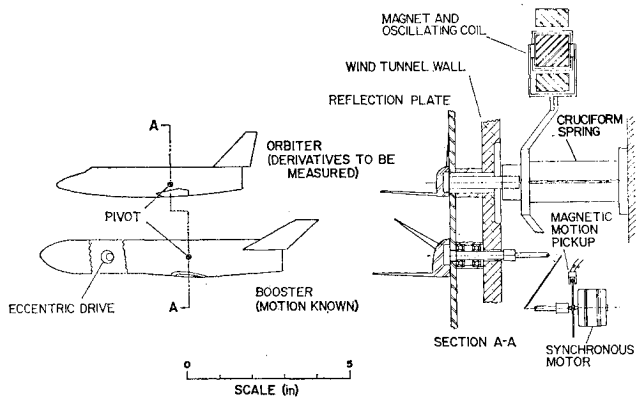

Fig. 1 Experimental arrangement for static and dynamic interference study on shuttle abort separation.

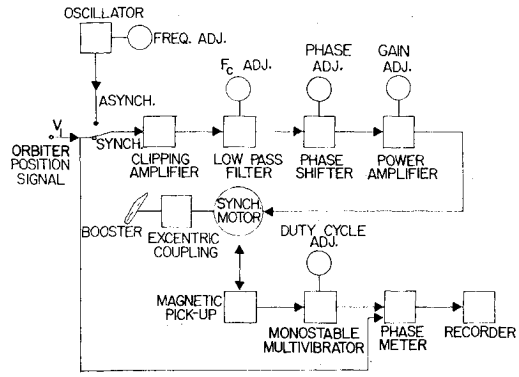

Fig. 2 Instrumentation for booster oscillation.

to the motor has a constant amplitude regardless of the amplitude of the oscillation of the orbiter; this is necessary for an optimum operation of the motor, which thus imparts a perfectly controlled motion to the booster.

The phase relationship between the motions of the two models can be adjusted by shifting the signal that drives the booster. The phase is determined by means of a phase meter connected between the displacement signal of the orbiter and a corresponding signal for the booster. The latter is generated with a magnetic pickup which produces a spike when the rotor of the motor is at a given position. For proper operation of the phasemeter, it is necessary to transform this signal into a more suitable waveform, which is accomplished by means of a monostable multivibrator with a 50% duty cycle.

Static Interference during Abort Separation

Static interference during abort separation is defined here as the interference on one of the component vehicles caused by the other vehicle which remains in the vicinity, and is stationary with respect to a system of coordinates moving with the center of gravity of the first vehicle. In this paper, we are mainly concerned with the static-interference effect caused by one vehicle on the damping-in-pitch characteristics of the other one. Consequently, experiments are described where the damping derivative was determined on the oscillating orbiter in the presence of the stationary booster and, vice versa, on the oscillating booster with the orbiter stationary. The experiments were conducted on both the straight-wing and the delta-wing shuttle configurations for a large number of relative positions of the two vehicles, and also for interference-free conditions. All measurements described in this section were performed at a Mach number of 1.80 and a Reynolds number of the order of 2.5 million, referred to the length of the booster.

An example of the interference-free values obtained is shown in Fig. 3, where the damping-in-pitch for the straight-wing orbiter alone is presented for several values of Reynolds number and angle-of-attack. It can be seen that the mean

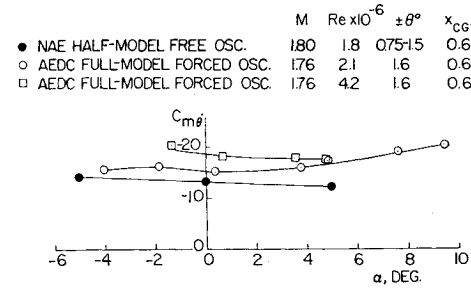

Fig. 3 Interference-free damping-in-pitch of the straight-wing orbiter.

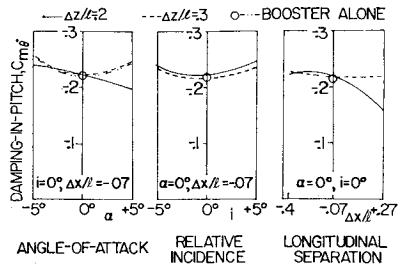

Fig. 4 Static-interference effect on the damping-in-pitch of the straight-wing booster, $M = 1.8$.

angle-of-attack has only a slight effect on the damping-in-pitch of the orbiter alone, while an increasing Reynolds number seems to increase that quantity in a moderate fashion. The NAE half-model free-oscillation data appear to be in very good agreement with the AEDC full-model forced-oscillation data (Ref. 5), especially when the effect of the difference in the amplitude of oscillation is taken into account. The corresponding dimensional damping-in-pitch ($C_{m\dot{\theta}} SI^2$) for the delta-wing orbiter has been found to be about 2.5 times larger than the data shown here for the straight-wing orbiter, while the corresponding ratio for the two boosters is about 4. The magnitude of the static-interference effect is illustrated in Fig. 4, where the damping-in-pitch for the straight-wing booster is shown for different locations of the nearby orbiter. The data are presented as functions of three separation and attitude variables with the fourth separation variable as parameter. The separation variables are: 1) the relative incidence i which is equal to the difference between the incidence of the orbiter and that of the booster, 2) the longitudinal separation Δx which is equal to the longitudinal distance of the *CG* of the orbiter behind the *CG* of the booster and 3) the vertical separation Δz, which is equal to the vertical distance of the *CG* of the orbiter above the *CG* of the booster. Both separation distances are referred to the length of the booster, l. The attitude variable, α, is the mean angle-of-attack of the model for which the damping derivative is presented. The variables α, i and $\Delta x/l$ are varied around a set of nominal conditions defined by $\alpha = i = 0°$ and $\Delta x/l = -0.07$. The static-interference effect is represented by the difference of the results plotted and the interference-free value which is indicated by a circle. It can be seen that this effect is everywhere relatively small; in both the case shown and in the reverse case of the static interference of the straight-wing booster on the damping-in-pitch of the orbiter, the maximum interference effect is 27% of the corresponding interference-free value. Detailed description of these experiments may be found in Ref. 1.

A similar investigation was performed on the delta-wing shuttle configuration (Ref. 2). Again, the static-interference effects were found to be relatively small. A comparison of these effects for the two configurations for several values of α and i is presented in Fig. 5. It may be concluded that the static-interference effect on the damping-in-pitch derivatives of the component shuttle vehicles is in general relatively small, and is not likely to significantly affect the dynamics of an abort-separation maneuver.

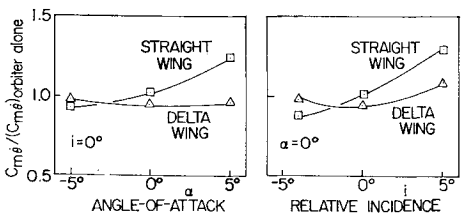

Fig. 5 Comparison of the static-interference effect on the orbiter damping-in-pitch for the two shuttle configurations; $M = 1.8$; $\Delta x/l \simeq -0.07$; $\Delta z/l \simeq 0.2$.

Oil-flow visualization studies were conducted in order to obtain detailed pictures of the interacting flow patterns over the two-model configuration at various separation attitudes. A 1:3 mixture of titanium dioxide and vacuum pump oil, and a small quantity of oleic acid were used for these experiments.

A typical photograph is shown in Fig. 6 with the straight-wing orbiter mounted well forward of the booster. A strong effect is visible of the booster bow shock on the orbiter body ahead of the wing, and of the leading-edge shock from the orbiter wing on the booster forebody. Also, the separation lines around the orbiter canopy and the interaction between the wing trailing-edge shock and the leading-edge shock of the horizontal stabilizer of the orbiter or the V-shaped stabilizer of the booster can be clearly seen.

As far as the flow on the reflection plate is concerned, one can observe the bow-shock-induced separation of the plate boundary layer and its subsequent reattachment and, in some cases, its secondary separation and secondary reattachment. These phenomena, however, seem to be confined to a layer immediately adjacent to the plate, and no effects of the plate boundary layer can be discerned on the flow characteristics over the bodies, wings or stabilizers of the two shuttle models. The interaction between the plate boundary layer and the various shock waves caused by the models can be observed as inflections in the plate streamlines, which may be used to study the propagation of these shock waves. The flow ahead of the models appears fully uniform everywhere with the possible exception of the area in the vicinity of the orbiter nose, where a slight disturbance associated with the very close edge (in this particular position) of the reflection plate can be discerned.

Dynamic Interference during Abort Separation

Dynamic interference during abort separation is defined as the interference on one of the component vehicles caused by the other vehicle which remains in the vicinity but, contrary to the static-interference case, performs some secondary motion with respect to a system of coordinates moving with the center of gravity of the first vehicle. The kind of secondary motion considered here is the oscillation in pitch, and attention is focused on the special case when this oscillation is synchronous with the oscillatory motion of the first vechicle, for which case the dynamic-interference effects may be expected to be particularly large. A study of the dynamic-interference effect of one of the vehicles on the damping-in-pitch characteristics of the other requires a wind-tunnel experiment where the damping derivative is measured on one oscillating model, while the other one performs a synchronous oscillatory motion with a known amplitude and an adjustable phase. Such experiments have now been performed on the delta-wing shuttle configuration. Since the interference effect could be assumed to vary with the size of the vehicle which causes it, the dynamic-interference effect of the booster on the damping derivative of the orbiter was expected to be larger than in the reverse situation, and was therefore investigated first. The material presented in this section is limited to that case, with all the

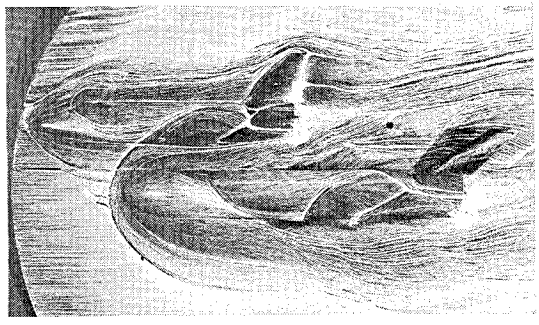

Fig. 6 Oil-flow visualization straight-wing shuttle in abort separation at Mach 1.8; $\Delta z/l = 0.2$; $\Delta x/l = -0.4$; $\alpha = i = 0°$.

experimental data obtained at a Mach number of 2.0, and for the relative position of the two vehicles defined by $i = 0$, $\Delta x/l = -0.06$ and $\Delta z/l = 0.19$.

The damping derivative of the delta-wing orbiter is shown in Fig. 7 as a function of the phase angle by which the orbiter leads the booster. The results are shown for two values of the nominal amplitude of the orbiter, while the amplitude of the booster was constant at 1.9°. The frequency of both vehicles was 47 Hz. Both the free-oscillation and the forced-oscillation method of measurements were employed, and the results are highly consistent. The pertinent interference-free value and the static-interference effect are also indicated in Fig. 7 for comparison. It was found that the dynamic-interference effect, i.e., the difference between the curves presented and the interference-free value, is up to two orders of magnitude larger than the static-interference effect and may result in values of the damping derivative which are between $+13$ and -8 times the interference-free value. Such large variation in damping and, especially, the occurrence of large negative damping (positive $C_{m\dot{\theta}}$), could have a significant effect on the flight dynamics of the orbiter. Should the two vehicles perform synchronous oscillation while in close proximity, and should the phase angle between the two motions be one for which a high negative damping has been observed, the abort-separation maneuver could be critically affected.

Since the orbiter is a much smaller vehicle than the booster, its natural frequency under normal interference-free conditions may be expected to be higher than that of the booster. However, it is shown in Fig. 8 that in the presence of dynamic interference the static pitching-moment derivative, and consequently the frequency of the orbiter, may be greatly reduced. (This derivative is presented here without any corrections for possible half-model effects, which are not likely to affect the present discussion). In the examples shown, which apply to the same experimental conditions as those of Fig. 7, this reduction is of the order of up to 50%, and does indeed occur in a range of phase angle that includes values for which negative damping has been measured. It appears, therefore, quite conceivable that conditions may arise during which the oscillatory flowfield of the booster forces the smaller orbiter to "lock-in" on the booster frequency, and at the same time, feeds enough energy into the orbiter to cause a rapidly diverging oscillation. If the procedure for abort separation is such that the two vehicles remain in proximity for a period of time during which several cycles of motion can take place, such a diverging oscillation of the orbiter may lead to a collision between the two vehicles.

It has to be kept in mind that all the experimental data presented here pertain to only one incidence ($\alpha = 0°$) and one relative position of the two vehicles, and that the dynamic interference effect certainly must be expected to be a strong function of these parameters. More experimental work is

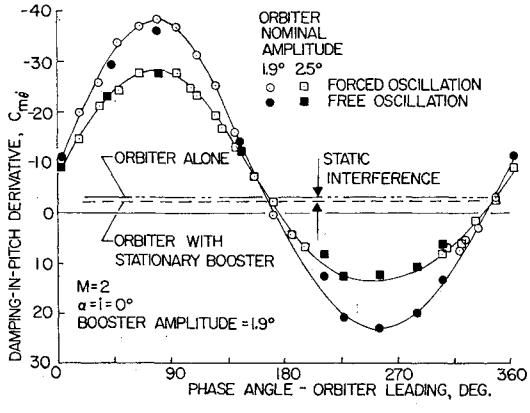

Fig. 7 Dynamic-interference effect on the damping-in-pitch of the delta-wing orbiter oscillating synchronously with the booster; $\Delta x/l = -0.06$; $\Delta z/l = 0.19$.

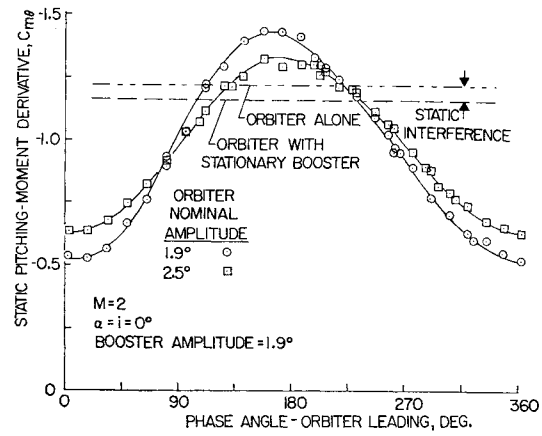

Fig. 8 Dynamic-interference effect on the static pitching-moment derivative of the delta-wing orbiter oscillating synchronously with the booster.

therefore needed, and this should include the determination of the effect of the incidence and the various separation variables, as well as a study of the dynamic-interference effect of the orbiter on the booster which, although probably much smaller, may still be significant. All these data should then be used in a realistic analysis of the flight mechanics problem involved.

The curves of Fig. 7 can be expressed in the approximate analytical form:

$$C_{m\dot{\theta}} = -5.39 - (76.0 - 22.6\theta) \sin(\psi + 13°)$$

where ψ is the phase angle by which the orbiter leads the booster and θ is the true amplitude of the orbiter. The expression for $C_{m\dot{\theta}}$ includes an approximate correction for the small deviation of the true amplitude from the nominal amplitude. This deviation was caused by an inadequacy of the stabilization system used, which resulted in amplitudes slightly too small in the presence of positive damping, and too large in the presence of negative damping. The θ-dependency was determined with the help of some additional points (not shown here) obtained at nominal amplitudes $\pm 1.2°$ and $\pm 2.2°$.

It may be seen from Figs. 7 and 8 that the dynamic-interference effect increases significantly when the amplitude of the orbiter decreases. This may be explained by the fact that the smaller the orbiter amplitude, the larger the ratio of the booster oscillatory energy to the orbiter oscillatory energy; this ratio may be expected to control the dynamic-interference phenomenon.

To obtain a better appreciation of the complex oscillating shock wave pattern during the dynamic-interference experiments, a high-speed shadowgraph motion picture has been made. To make it possible to use optical techniques with half-model experiments, a flat front-surface mirror was inserted into the reflection plate, and an optical window was mounted into a specially prepared circular cutout in the Mach 2 nozzle liner on the tunnel wall opposite to the half-model dynamic balance. A single frame from the motion picture is reproduced in Fig. 9.

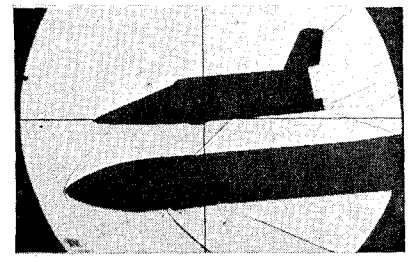

Fig. 9 Frame from shadowgraph high-speed motion picture of delta-wing orbiter and booster in synchronous oscillation; $M = 2$.

Launch Configuration with and without Plume Interference

Proper knowledge of the damping derivatives may be particularly important during the ascending flight of the shuttle, when the destabilizing effect of the negative density gradient may render the vehicle quite sensitive to its inherent aerodynamic stability characteristics. An analytical determination of the damping derivatives for a configuration as complex as the mated launch configuration is, of course, extremely complicated. In addition, during the ascending portion of the flight, the rocket-exhaust plume, which oscillates together with the vehicle, may also influence to some extent the aerodynamic stability characteristics of the vehicle, including its aerodynamic damping. An experimental determination of the damping derivative of the launch configuration, including a study of the plume-interference effect, is therefore highly desirable.

The previously described (Fig. 1) experimental arrangement and delta-wing shuttle models were modified in order to allow simulation of the rocket-exhaust plume on an oscillating model of the mated launch configuration.[6] A high-pressure nitrogen supply line was incorporated, in a frictionless fashion, in the half-model dynamic balance, and an adapter containing a high-pressure chamber and an exhaust nozzle was inserted in the body of the booster. The half-model technique is eminently suitable for such an investigation since it eliminates entirely the large reaction which may be expected to exist between the oscillating plume and the stationary sting of a conventional sting support. It also makes possible, without any problems, the correct positioning of the center of oscillation of the mated launch configuration.

As may be seen from Fig. 10, the damping-in-pitch derivative of the launch configuration decreases with increasing supersonic Mach number, while its variation with angle of attack is far less pronounced. The information presented here is for the delta-wing shuttle oscillating with an amplitude of $\pm 2.5°$. Similar data for the booster alone at Mach 1.8 (but oscillating around an axis which is located slightly more rearward) are included for comparison. It appears that the addition of a piggy-back orbiter has only a small effect on the damping derivative. The positions of the axis of oscillation are given by x_{CG}/l and z_{CG}/l, which are distances behind the booster nose and above the booster C.G., respectively, both expressed in terms of the booster length. These positions represent approximately the centers of gravity of the full-scale vehicles during the low-supersonic portion of the ascent trajectory.

The simulation of the shape and size (but not necessarily the momentum) of the exhaust plume was achieved by duplicating the nozzle-exit wall angle, the initial plume boundary angle, and the ratio of the initial plume boundary Mach number to the specific heat ratio. Thus, using dry nitrogen at 1500 psi, nozzle wall angle of 14° and nozzle area-ratio of 11.9 (exit Mach number of 4.1), the full-scale conditions were simulated of a booster with nozzle area-ratio of 34, flying at Mach 2 at 63,000 ft, and with 50% thrust level (1500 psi chamber pressure). One nozzle only was used on the half-model with a throat area corresponding to one-half of the scaled-down total throat area on the full-scale vehicle.

The reflection plate was extended (by installing an extra flat plate which was removable for calibration) in the downstream direction, and oil-flow visualization was employed to confirm the shape and the size of the exhaust plume. The conditions on the photograph in Fig. 11 represent flow at Mach 2 and the nozzle exit to freestream pressure ratio of 6.5, which was close to the highest pressure ratio tested. Streamlines on the model are also visible. No oil was applied to the main part of the reflection plate.

Plume-interference effect on the damping-in-pitch derivative was obtained from the following expression:

$$\Delta(C_{m\dot{\theta}})_{\text{plume interference}} = (C_{m\dot{\theta}})_{\text{plume net}} - (C_{m\dot{\theta}})_{\text{no plume}}$$

where

$$(C_{m\dot{\theta}})_{\text{plume net}} = (C_{m\dot{\theta}})_{\text{plume gross}} - \Delta(C_{m\dot{\theta}})_{\text{plate, plume}} - \Delta(C_{m\dot{\theta}})_{\text{jet, vac.}}$$

where $(C_{m\dot{\theta}})_{\text{plume gross}}$ and $(C_{m\dot{\theta}})_{\text{no plume}}$ are the usual damping derivatives, measured with and without the plume, respectively, and the $\Delta(C_{m\dot{\theta}})$ terms are calibration terms obtained with no flow in the tunnel but expressed here, for convenience, in the form of equivalent derivatives. $\Delta(C_{m\dot{\theta}})_{\text{jet, vac.}}$ represents the internal effect of the nitrogen flow inside the model, and was determined from the difference in damping measured in vacuum with and without the jet. $\Delta(C_{m\dot{\theta}})_{\text{plate, plume}}$ represents the effect of the reflection plate on the plume, and was obtained at a pressure equal to the static pressure during a run from a difference in damping measured with and without the reflection plate extension.

Experimental results, shown in Fig. 12, indicate that the plume interference effect on the damping-in-pitch derivative is quite small, of the order of 15% at the design point for the configuration tested. The effect of the internal nitrogen flow, however, is significantly larger and, although this quantity was not simulated in the present experiments, it may be worth considering for a full-scale rocket-engine flow. The effect of the reflection plate extension on the plume is negligible (too small to be shown), confirming the suitability of half-model oscillatory techniques for this type of experiment.

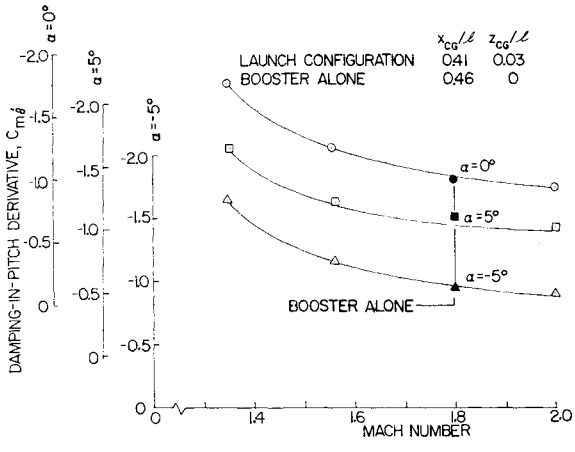

Fig. 10 Effect of Mach number on the damping-in-pitch of the delta-wing launch configuration.

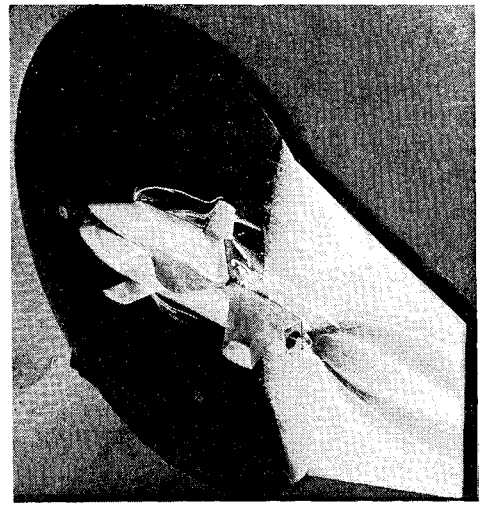

Fig. 11 Oil-flow visualization; launch configuration of delta-wing shuttle with simulated exhaust plume at Mach 2 and $\alpha = 0°$.

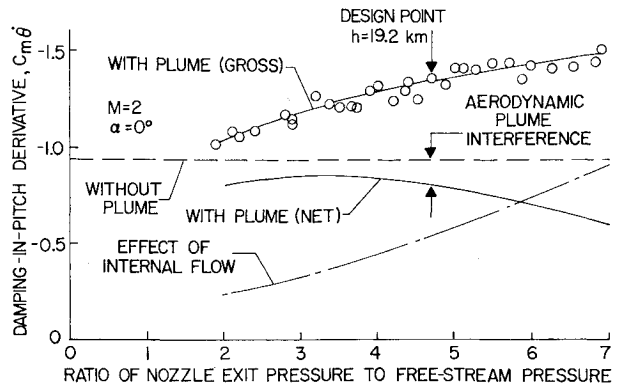

Fig. 12 Plume-interference effect on damping-in-pitch of delta-wing launch configuration.

Conclusions

In the range of experimental conditions investigated, the following applies: 1) Interference-free dimensional damping is substantially higher for the delta-wing than for the straight-wing shuttle configuration. 2) For both configurations during abort separation, the static-interference effects on damping are relatively small. 3) For the two vehicles in synchronous oscillation, the dynamic-interference effects are very large and may lead to negative damping conditions. The possibility of the orbiter "locking-in" with the oscillatory flowfield of the booster and developing rapidly diverging oscillation that could lead to collision during abort separation cannot be ruled out, and should be investigated further. More experimental data, as well as a realistic flight mechanics analysis, are needed. 4) The damping of the delta-wing launch configuration and of the booster alone are of the same order of magnitude. 5) Plume-interference effects on damping appear to be small. 6) The half-model technique appears to be uniquely suitable for oscillatory experiments involving two models in simultaneous motion and models with simulated plume effect.

References

[1] Orlik-Rückemann, K. J. and LaBerge, J. G., "Dynamic Stability Experiments on Straight-Wing Space Shuttle in Abort Separation at $M=1.80$," NAE LTR-UA-16, May 1971, National Research Council of Canada, Ottawa, Ontario, Canada.

[2] LaBerge, J. G., "Dynamic Stability Experiments on Delta-Wing Shuttle in Abort Separation at $M=1.80$," NAE LTR-UA-17, July 1971, National Research Council of Canada, Ottawa, Ontario, Canada.

[3] Orlik-Rückemann, K. J. and LaBerge, J. G., "Dynamic Interference Effect on Dynamic Stability of Delta-Wing Shuttle in Abort Separation at $M=2.0$," NAE LTR-UA-18, Nov. 1971, National Research Council of Canada, Ottawa, Ontario, Canada.

[4] Orlik-Rückemann, K. J., Adams, P. A., and LaBerge, J. G., "Dynamic Stability Testing of Unconventional Configurations," *Journal of Aircraft*, Vol. 9, No. 2, Feb. 1972, pp. 101–102.

[5] Uselton, R. and Wallace, A. R., "Dynamic Stability Testing of Space Shuttle Configurations During Abort Separation at Mach Numbers 1.76 and 2," TR-71-198, Oct. 1971, Arnold Engineering Development Center, Arnold Air Force Station, Tenn.

[6] LaBerge, J. G. and Orlik-Rückemann, K. J., "Aerodynamic Plume Interference on the Damping-In-Pitch of the Delta-Wing Shuttle Launch Configuration at Supersonic Speeds," NAE LTR-UA-20, June 1972, National Research Council of Canada, Ottawa, Ontario, Canada.

SEPTEMBER 1972 J. SPACECRAFT VOL. 9, NO. 9

Entry Probe Descent to the Base of the Jovian Clouds

HOWARD B. WINKLER,* DONALD P. FIELDS,† RUSSELL G. GAMACHE‡
Avco Corporation/Systems Division, Wilmington, Mass.

A study was conducted to identify and describe feasible first-generation Jupiter entry probe missions that measure atmospheric phenomena below the cloud tops, and that tend to minimize engineering development. A principal groundrule for this study has been entry probe survival to the base of the cloud layer with remote sensing to provide information at greater atmospheric depths. The major tradeoffs that were considered include 1) entry probe release from a 1978 and 1980 flyby trajectory, and from a 1979 Grand Tour trajectory, 2) use of a TOPS or Pioneer F/G as an interplanetary bus, 3) direct and relay communication links, and 4) dayside and nightside entry. Many feasible missions were identified; use of remote sensing would extend the downward "reach" of the entry probe.

Introduction

THE approach taken for the investigation of a first-generation Jupiter atmospheric entry probe was to identify the key science and engineering tradeoffs. These tradeoff studies were intended to reveal those missions that combine good science with favorable engineering. Entry probe supporting systems and subsystem configurations were generated based on favorable mission combinations.

A principal groundrule for this study has been entry probe survival to the base of the cloud layer with remote sensing to provide information at greater atmospheric depths. This approach to the study of a Jupiter atmospheric entry probe mission is significantly different from the equally valid approach of entry probe survival to great depths within the atmosphere with in situ sensing. Descent to the cloud base eases the entry probe engineering design and development requirements. For example, in the nominal Jovian atmos-

Presented as Paper 71-834 at the AIAA Space Systems Meeting; Denver, Colo., July 19–20, 1971; submitted August 12, 1971; revision received April 17, 1972. This work was performed for the Jet Propulsion Laboratory, California Institute of Technology sponsored by NASA under Contract NAS 7-100. The authors would like to acknowledge the science contribution of J. S. Lewis, Assistant Professor of Chemistry and Geochemistry, Massachusetts Institute of Technology.

Index category: Entry Vehicle Mission Studies and Flight Mechanics.

* Study Leader, Senior Consulting Engineer. Associate Fellow AIAA.

† Lead Engineer, Section Chief of Mission Analysis and System Performance.

‡ Lead Engineer, Group Leader of Communication Analysis.